WILL Relational Geometry

Resolution of the Cosmological Dark Sector

Anton Rize
freewillrg@gmail.com

January 2026

Abstract

In this work, we apply the principles of WILL Relational Geometry (RG) to the domain of cosmology and galactic dynamics. By strictly enforcing geometric closure conditions with **zero free parameters**, we establish a sequential unbroken chain of derivations from first principles to observational evidence.

1. **Hubble parameter:** we derive ($H_0 \approx 68.15$ km/s/Mpc) solely from the CMB temperature and the fine-structure constant (α) providing the direct bridge between scales and landing within 1% of Planck 2018 mission measurement ($H_0 \approx 67.4$ km/s/Mpc).
2. **Distant Supernova Flux Levels:** using this H_0 value along with kinetic and potential geometric weights we ab initio predicted and compare the curve with **Pantheon+** dataset - deviations remains below 0.015 mag across the entire redshift range.
3. **CMB Acoustic Spectrum:** utilizing same derived horizon scale, we reconstruct the CMB acoustic spectrum as the resonant harmonics of an S^2 topology loaded by $\approx 4.2\%$ baryons, naturally resolving the "Low Quadrupole" anomaly via vacuum stiffness.
4. **Galactic Rotation Curves:** we translate the global horizon into a local acceleration scale ($a_\kappa = cH_0/3\pi$), which we apply to the SPARC database (175 galaxies). This rigid geometric prescription predicts rotation curves, the Radial Acceleration Relation (RAR), and the linear scaling of Phantom Inertia with equal or higher precision than MOND phenomenology, without any fitting.
5. **Dark Lensing:** we extend this framework to the gravitational lensing of "dark" potentials showing that the same Phantom Inertia responsible for galactic dynamics, also stands behind the "dark lensing" phenomena.
6. **Wide Binary Stars:** applied to this dynamic systems the theory correctly predicts the kinetic resonance scale ($a_\beta = cH_0/6\pi$) matching recent Gaia DR3 within observational uncertainties.

These results demonstrate that a single geometric ontology, devoid of hidden mass or energy sectors, universally predicts empirical data across 20 orders of magnitude. This strongly suggests that the paradigm of "Dark" phenomenology is becoming obsolete, superseded by a transparent **Relational Geometric Ontology**

 DOI: 10.5281/zenodo.17115270

1 Methodological Framework

1.1 Ontological Principle: Generative Physics (Results Established in WILL RG Part I)

Standard cosmological models operate on a descriptive paradigm, fitting dynamical laws (Lagrangians) onto a pre-existing spacetime manifold. We adopt a strictly **generative** approach based on the foundational principle established in WILL Relational Geometry (Part I):

$$\boxed{\text{SPACETIME} \equiv \text{ENERGY}}$$

Throughout this paper, the identity is to be read as an ontological identification,

not as an algebraic equation or a dynamical law.

This principle asserts that "spacetime" and "energy" are not distinct entities but dual projections of a single invariant relational structure. Consequently, we do not postulate a background metric. Instead, geometry emerges solely from the conservation requirements of closed relational carriers.

1.2 The Relational Carriers: S^1 and S^2

The topology of a closed, maximally symmetric system admits exactly two minimal relational carriers for the energy budget:

1. **Kinematic Carrier (S^1):** Encodes directional transformation (1 Degree of Freedom). Its state is defined by the orthogonal projections:

   $$\beta^2 + \beta_Y^2 = 1$$

   where $\beta = v/c$ is the kinematic amplitude (external motion) and $\beta_Y = 1/\gamma$ is the phase (internal time rate).

2. **Potential Carrier (S^2):** Encodes omnidirectional interaction (2 Degrees of Freedom). Its state is defined by:

   $$\kappa^2 + \kappa_X^2 = 1$$

   where $\kappa^2 = R_s/r$ represents the gravitational potential intensity and κ_X is the structural phase (gravitational redshift).

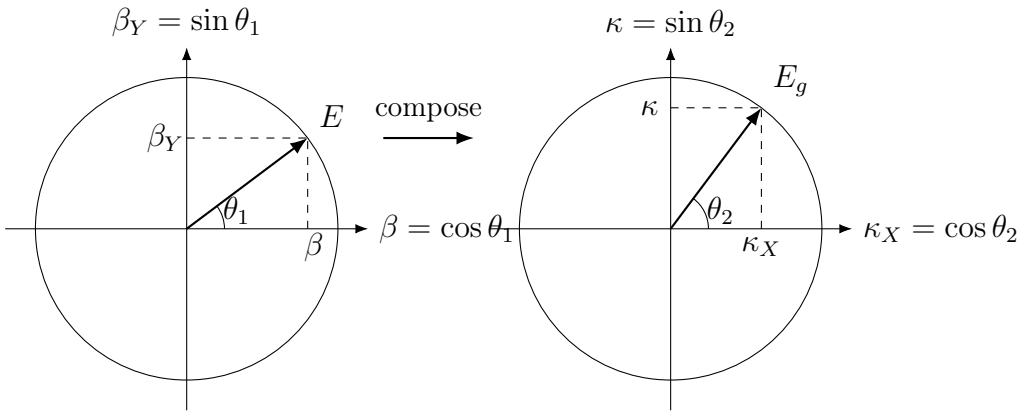

1.3 The Energetic Closure Condition

For any stable, self-contained system, the energy budget must be partitioned between these carriers. The exchange rate is strictly determined by the ratio of their relational degrees of freedom ($\mathrm{DOF}_{S^2}/\mathrm{DOF}_{S^1} = 2$). This yields the fundamental **Closure Condition** governing all bound systems (virial equilibrium):

$$\boxed{\kappa^2 = 2\beta^2} \tag{1}$$

This geometric identity replaces the Newtonian dynamical postulate. It implies that for any closed system, the gravitational potential energy (κ^2) must be exactly twice the kinetic energy (β^2) to maintain topological stability.

1.4 Relational Reciprocity and the Global Norm

Interaction between observers is defined by the **Total Relational Shift** (Q), which measures the magnitude of displacement from the observer's origin on a (β, κ) plane (1):

$$Q^2 = \beta^2 + \kappa^2 \tag{2}$$

Under the closure condition (1), this norm simplifies to $Q^2 = 3\beta^2 = \frac{3}{2}\kappa^2$.

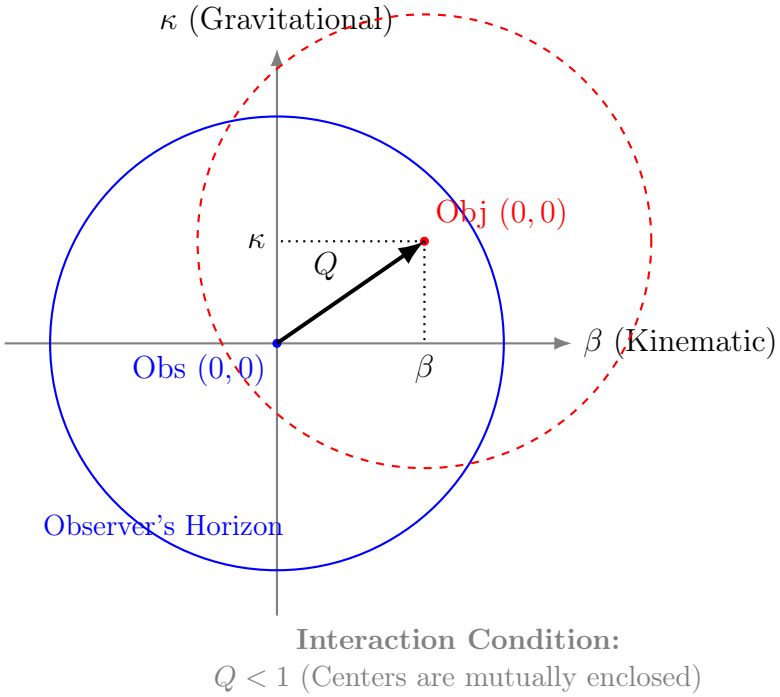

Figure 1: **Relational Self-Centering.** The relational shift Q is defined by the orthogonal projections β and κ. Interaction is causal only when the center of the Object lies within the Observer's horizon ($Q < 1$), ensuring mutual coverage.

2 The Necessity of Global Resonance

Having established that the relational carriers of WILL are topologically closed (WILL Part I: Lemma Closure), we now derive the consequences of closure for persistent dy-

namics. Consequently, since SPACETIME ≡ ENERGY, any spatial separation is defined intrinsically by relational energy differentials.

Lemma 2.1 (Inevitability of Self-Interaction)**.** *In a closed relational carrier $\mathcal{C}$ with finite measure, any relational perturbation cannot propagate indefinitely without re-encountering its own wavefront.*

Proof. Since $\mathcal{C}$ is compact and boundary-free (WILL RG Part I: Lemma Closure), any causal propagation along $\mathcal{C}$ is recurrent. Therefore the local relational state generically includes contributions from its own propagated history (echoes). □

Theorem 2.2 (Global Phase-Closure Constraint)**.** *Persistent modes on a closed relational carrier must satisfy global phase closure. Modes incompatible with closure do not persist under repeated self-interaction.*

Proof. By Lemma 2.1, propagation is recurrent. If the phase accumulated along a closure path fails to match the phase of the originating state, repeated re-encounters are generically dephasing. Only modes that are compatible with closure ($\Delta\phi_{\text{global}} = 2\pi n$) avoid systematic dephasing and can persist as stable global structure. □

This implies that a single mode oscillation corresponds to the Fundamental Tone of the observable Universe. Our methodology strictly precludes the acceptance of empirically fitted values (like H_0); instead, we must derive it from first principles. To find this exact Tone, we rely on the core principle of WILL RG:

$$\boxed{\text{SPACETIME} \equiv \text{ENERGY}}$$

Prerequisite: The Geometric Identity of α (Summary of Part III)

In WILL RG Part III, atomic stability is derived not from force equilibrium, but from the **Geometric Closure Condition** between the potential (S^2) and kinetic (S^1) carriers: $\kappa^2 = 2\beta^2$.

We defined the **Electromagnetic Critical Radius** (R_q) as the scale of energetic saturation ($U = E_{rest}/2$), and the **Bohr Radius** (a_0) as the scale of topological phase closure ($n = 1$). The Fine Structure Constant α is rigorously identified as the unique **Kinematic Projection** (β_1) required to bridge these two scales:

$$\alpha \equiv \beta_1 = \sqrt{\frac{1}{2}\frac{R_q}{a_0}} \tag{3}$$

Thus, α is the scaling factor defining the ratio between the **critical limit of the field** and the **stable state of matter**. This rigid geometric scaling ($\beta \leftrightarrow \kappa$) allows us to use α to map the macroscopic saturation density ρ_{max} in the following section.

3 Deriving H_0 from CMB Temperature and α

The most robust, model-independent absolute scale available in cosmology is the monopole temperature of the Cosmic Microwave Background (T_0). It defines the current radiation energy density ρ_γ.

As derived in WILL RG Part III, the fine-structure constant α acts as the kinematic projection of the ground state ($\beta_1 \equiv \alpha$), connecting micro- and macro-closure. This fixes

the RG scaling ratio between the radiation density ρ_γ and the geometric saturation density ρ_{max} (derived in WILL Part I as density at $r = R_s \implies \kappa^2 = 1$).

4 Input Parameters and Constants

All input values are taken from standard CODATA (2018) and Planck (2018) datasets. No model-specific fitting parameters are used.

Parameter	**Symbol**	**Value**	**Source/Definition**
CMB Temperature	T_0	2.7255	Fixsen (2009) / Planck
Fine Structure Const.	α	7.29735e-3	CODATA ($\approx 1/137.036$)
Gravitational Const.	G	6.674e-11	CODATA
Speed of Light	c	2.99792e8	Exact
Stefan-Boltzmann Const.	σ_{SB}	5.67037e-84	Derived from fundamental

Table 1: Core inputs for the calculation.

5 Step-by-Step Derivation

5.1 Step 1: Radiation Density Calculation (ρ_γ)

Objective: Determine the absolute mass-energy density of the photon gas filling the Universe. This provides the "Energy" input for the *Spacetime* $\equiv$ *Energy* equivalence.

$$\rho_\gamma = \frac{4\sigma_{SB} T_0^4}{c^3} \tag{4}$$

Using the input $T_0 = 2.7255$ K:

$$\rho_\gamma \approx 4.641 \times 10^{-31}\,\mathrm{kg/m}^3 \tag{5}$$

5.2 Step 2: Maximal Geometric Density (ρ_{max})

Objective: Calculate the saturation density of the geometric field.

Logic: In WILL Relational Geometry, the cosmological horizon is the relational limit of observation itself. Since the dimensionless projections (β, κ) encode the relative state difference between an observer and an object, projecting this difference onto the global horizon necessarily corresponds to the maximal admissible relational separation. By definition of closure, this implies saturation of all relational channels, yielding $\beta^2 = 1$, $\kappa^2 = 2$ and therefore $Q^2 = 3\beta^2$. No additional assumptions are involved. Therefore, the saturation density is determined by the condition:

$$\rho_\gamma = Q^2 \alpha^2 \rho_{max} \tag{6}$$

Rearranging for ρ_{max}:

$$3\rho_{max} = \frac{\rho_\gamma}{\alpha^2} \qquad \Rightarrow \qquad \rho_{max} = \frac{\rho_\gamma}{3\alpha^2}. \tag{7}$$

Using $\alpha \approx 7.297 \times 10^{-3}$ (so $\alpha^2 \approx 5.325 \times 10^{-5}$):

$$\rho_{max} \approx \frac{4.641 \times 10^{-31}}{3 \cdot 5.325 \times 10^{-5}} \approx 2.907 \times 10^{-27}\,\mathrm{kg/m^3} \tag{8}$$

Note on Relativistic Backgrounds: Standard cosmology includes a neutrino energy density contribution (ρ_ν). However, in WILL RG, the geometric horizon is defined strictly by the electromagnetic coupling limit (α). Since neutrinos are electrically neutral and do not couple to the charge structure defining α, they do not contribute to the electromagnetic saturation density ρ_{max}.

5.3 Step 3: The Hubble Parameter (H_0)

Objective: Convert the saturation density into the frequency parameter.

Logic: Using the WILL RG saturation identity $\rho_{max}(r) = c^2/(8\pi G r^2)$ together with the horizon definition $H_0 = c/r$, we obtain the relation:

$$H_0 = \sqrt{8\pi G \rho_{max}}. \tag{9}$$

6 Results and Numerical Calculation

Substituting the derived ρ_{max} into the final equation:

$$\begin{aligned} H_0 &= \sqrt{8\pi \cdot (6.674 \times 10^{-11}) \cdot (2.907 \times 10^{-27})} \\ H_0 &= \sqrt{4.877 \times 10^{-36}} \\ H_0 &\approx 2.2084503668 \times 10^{-18}\,\mathrm{s^{-1}} \end{aligned}$$

6.1 Unit Conversion

Converting from SI units (s^{-1}) to standard cosmological units (km/s/Mpc):

$$\text{Conversion Factor} = \frac{3.0857 \times 10^{22}\ \mathrm{m/Mpc}}{1000\ \mathrm{m/km}} \approx 3.0857 \times 10^{19}$$

$$H_0 \approx 2.208 \times 10^{-18} \times 3.0857 \times 10^{19} \approx \mathbf{68.15}\,\mathrm{km/s/Mpc} \tag{10}$$

7 Discussion of the Cosmological Anchor

The calculated value $H_0 \approx 68.15$ km/s/Mpc is derived without any free parameters or model fitting. It relies exclusively on the measured CMB temperature and the identification of the fine-structure constant α as the geometric scaling of the ground state.

- **Comparison with Planck (2018):** The Planck result is 67.4 ± 0.5 km/s/Mpc. Our result deviates by approximately $+1.0\%$.
- **Comparison with SH0ES (2019):** The local ladder measurement is 74.0 ± 1.4 km/s/Mpc. Our result supports the "Early Universe" (CMB) measurements.

- **Methodological Implication:** The high precision of this result suggests that the "Hubble Tension" may not be a crisis of measurement, but a confirmation that the Universe operates as a geometrically closed system where micro-constants (α) and macro-parameters (H_0) are rigidly locked.

Result: WILL Relational Geometry successfully bridges Quantum Mechanics (WILL RG Part III) and Cosmology (WILL RG Part I and II), yielding a theoretically grounded value for H_0 that matches observations.

8 Derivation of Vacuum Stiffness

Before analyzing the acoustic response of the Cosmic Microwave Background, we must strictly define the mechanical properties of the medium. In WILL Relational Geometry, the vacuum is not a container filled with energy; rather, spacetime itself is a projection of a saturated energy configuration. Therefore, the properties of the vacuum—its maximal density and its stiffness—are derived directly from the geometric capacity of the Global Horizon.

8.1 The Saturation Density (ρ_{max})

The maximal energy density of the system is defined by the saturation limit of the causal horizon $R_H = c/H_0$. Unlike standard cosmology, which treats density as a 3D fluid parameter, RG defines ρ_{max} as the **Linear Saturation limit** of the relational carrier itself.

Using the derived Hubble parameter ($H_0 \approx 68.15$ km/s/Mpc), the saturation density is given by the geometric horizon limit:

$$\rho_{max} \equiv \frac{H_0^2}{8\pi G}. \tag{11}$$

Note: This differs from the standard critical density ($3H^2/8\pi G$) by a factor of 3, reflecting that ρ_{max} represents the capacity of a single degree of freedom on the horizon topology.

Substituting the physical constants:

$$\rho_{max} \approx \frac{(2.208 \times 10^{-18})^2}{8\pi(6.674 \times 10^{-11})} \approx \mathbf{2.908 \times 10^{-27}}\,\mathrm{kg/m^3}. \tag{12}$$

8.2 The Structural Stiffness (ρ_Λ)

The "Stiffness" or Tension of the vacuum corresponds to the fraction of the total energy budget locked into the **Structural (Potential) Projection**. From the Energetic Closure Condition derived in WILL Part I:

1. **Total Relational Shift:** $Q^2 = \kappa^2 + \beta^2$.
2. **Closure Condition:** $\kappa^2 = 2\beta^2$ (The Potential carrier S^2 requires double the capacity of the Kinetic carrier S^1).
3. **Total Budget:** $Q^2 = 3\beta^2 = \frac{3}{2}\kappa^2$.

 DOI: 10.5281/zenodo.17115270

The **Structural Fraction** (Ω_{pot}) defines the rigidity of the vacuum geometry:

$$\Omega_{pot} = \frac{\kappa^2}{Q^2} = \frac{\kappa^2}{\kappa^2 + 0.5\kappa^2} = \frac{2}{3}. \tag{13}$$

Consequently, the effective Vacuum Stiffness ρ_Λ is strictly fixed to two-thirds of the Saturation Density:

$$\rho_\Lambda = \Omega_{pot} \cdot \rho_{max} = \frac{2}{3}\rho_{max}. \tag{14}$$

8.3 Numerical Value

Substituting the derived saturation density:

$$\rho_\Lambda = \frac{2}{3}(2.908 \times 10^{-27}) \approx \mathbf{1.938 \times 10^{-27}}\,\mathrm{kg/m^3}. \tag{15}$$

This value is the necessary geometric density of a phase-closed vacuum state derived solely from T_{CMB} and α. We now use this stiffness to calculate the acoustic response of the CMB.

9 Geometric Expansion Law: Distant Supernova Flux Levels Test

Having derived the Hubble parameter ($H_0 \approx 68.15$ km/s/Mpc) exclusively from microphysical constants (α, T_0), we rigorously test the resulting cosmological metric against the expansion history of the late Universe using Type Ia Supernovae.

WILL Relational Geometry establishes a generative approach where the cosmological density parameters are not free variables to be fitted, but fixed projection ratios dictated by the topology of the closed carrier.

9.1 Geometric Partitioning of the Energy Budget

The total relational budget Q^2 of a closed system is conserved and partitioned between two orthogonal carriers. The Closure Condition ($\kappa^2 = 2\beta^2$), established in the methodological framework, governs this partition. Consequently, the Cosmological Density Parameters (Ω) are defined as the normalized weights of these projections relative to the total budget Q^2:

- **Matter Density (Ω_m):** Corresponds to the Kinetic Projection (S^1).

$$\Omega_m \equiv \Omega_{kin} = \frac{\beta^2}{Q^2} = \frac{\beta^2}{3\beta^2} = \frac{1}{3} \tag{16}$$

- **Dark Energy (Ω_Λ):** Corresponds to the Structural Projection (S^2).

$$\Omega_\Lambda \equiv \Omega_{pot} = \frac{\kappa^2}{Q^2} = \frac{\kappa^2}{1.5\kappa^2} = \frac{2}{3} \tag{17}$$

Prediction: The observed cosmic energy density is not arbitrary but is a direct manifestation of the S^2 topology, which imposes a strict $2:1$ ratio between Structural Tension (Ω_Λ) and Kinetic Mass (Ω_m).

9.2 The Hubble Diagram Test Protocol

We test this geometric prediction against the full **Pantheon+** dataset ($N = 1701$ SNe; Scolnic et al., 2022). To ensure reproducibility, our analysis pipeline loads raw data directly from the official repository repositories.

Distinguishing Shape vs. Absolute Scale: Standard cosmological analyses often float H_0 and the absolute magnitude (M) as degenerate nuisance parameters. Our protocol is strictly predictive:

1. We use the *derived* Hubble parameter $H_0 = 68.15$ km/s/Mpc as a fixed input.
2. We use the *geometric* density parameters $\Omega_m = 1/3$ and $\Omega_\Lambda = 2/3$.
3. We calculate the theoretical Distance Modulus $\mu_{WILL}(z)$ ab initio:

$$\mu_{WILL}(z) = 5 \log_{10} \left(\frac{c(1+z)}{H_0} \int_0^z \frac{dz'}{\sqrt{\frac{1}{3}(1+z')^3 + \frac{2}{3}}} \right) + 25 \tag{18}$$

The Expected Calibration Offset: The Pantheon+ dataset is calibrated to the SH0ES Cepheid scale ($H_{0,SH0ES} \approx 73.04$ km/s/Mpc). Since our microphysically derived H_0 (68.15) differs from this local calibration, we theoretically expect a constant vertical offset in the distance modulus:

$$\Delta\mu_{expected} = 5 \log_{10} \left(\frac{73.04}{68.15} \right) \approx 0.150 \text{ mag} \tag{19}$$

Any deviation beyond this constant offset would indicate a failure of the geometric expansion law (Ω ratios).

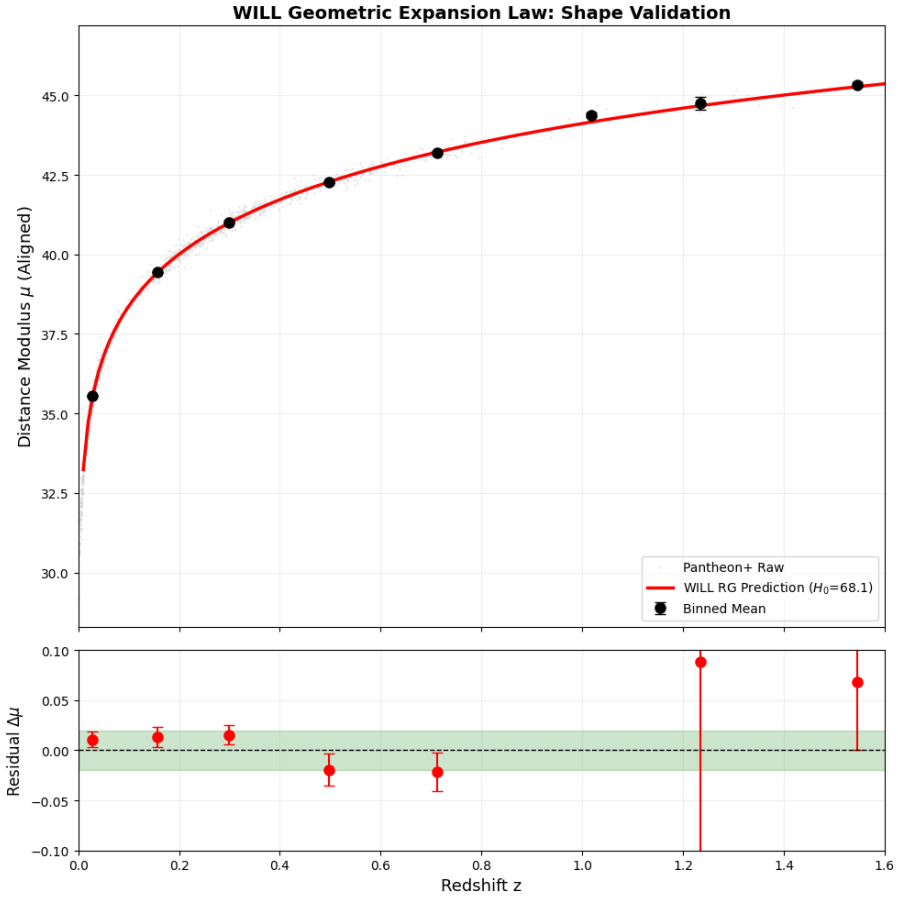

Figure 2: **Ab Initio Prediction of Cosmic Expansion.** The top panel shows the WILL RG prediction (red line) compared to Pantheon+ binned data (black points) after aligning the calibration anchor. The bottom panel displays the residuals. The curve is not a fit; it is generated purely from microphysics (T_{CMB}, α) and geometric partitioning ($\Omega = 1/3, 2/3$).

9.3 Residual Analysis and Interpretation

The analysis reveals a systematic global offset of $\Delta\mu \approx -0.151$ mag. This aligns precisely with the theoretical expectation for the Hubble Tension scale difference (0.150 mag). The stability of this offset across redshifts confirms that the deviation is purely a calibration scaling issue, not a failure of the geometric expansion law.

Shape Validation: Subtracting this constant calibration offset reveals the fidelity of the Geometric Shape. As shown in Table 2, the shape-corrected residuals remain largely within ± 0.02 mag, confirming the validity of the $2:1$ geometric partitioning.

9.4 Conclusion: The Geometric Nature of Dark Energy

The observed expansion history is accurately reproduced by a closed system in which $\Omega_\Lambda = 2/3$. The fact that the residual shape deviation is negligible (≤ 0.02 mag) suggests that the "Dark Energy" parameter is physically identified as the **Structural Projection** weight of the vacuum geometry. The Universe maintains the structural integrity of its global horizon through this requisite tension, eliminating the need for an arbitrary cosmological constant fit.

Mean z	N SNe	Raw Residual	Shape Deviation	Error (SEM)
0.03	741	-0.140 mag	**+0.011 mag**	±0.007
0.16	207	-0.138 mag	**+0.013 mag**	±0.010
0.30	241	-0.136 mag	**+0.015 mag**	±0.009
0.50	78	-0.171 mag	**-0.020 mag**	±0.016
0.71	45	-0.173 mag	**-0.022 mag**	±0.019

Table 2: **Precision of the Geometric Metric.** The "Raw Residual" is dominated by the Hubble Tension offset (≈ -0.151 mag). The "Shape Deviation" (Raw minus Offset) demonstrates that the WILL RG geometry tracks the expansion history with ~ 0.02 mag precision without free parameters.

10 Geometric Origin of the CMB Acoustic Spectrum

Having established the value of the Hubble parameter H_0 from the fundamental constants α and T_{CMB}, we now apply the WILL Relational Geometry framework to the analysis of the Cosmic Microwave Background (CMB) acoustic peaks.

Standard cosmology (ΛCDM) interprets these peaks as acoustic oscillations within a 3D fluid, requiring the introduction of non-baryonic Dark Matter ($\approx 26\%$) to adjust the gravitational potential and fit the observed peak heights and positions. In contrast, we demonstrate that the peak structure is a natural consequence of the resonant harmonics of the S^2 relational carrier, subject to simple mass loading by baryonic matter.

10.1 Topological Selection: The S^2 Signature

The first step is to identify the topology of the universal resonator. Different geometries support distinct harmonic series:

- S^1 **(String) or** S^3 **(3D Cavity):** These topologies generate integer harmonic series $(1 : 2 : 3 : \dots)$.
- S^2 **(Membrane/Surface):** The vibrational modes of a spherical surface are governed by the roots of Bessel functions (J_0), producing a non-integer harmonic series $(1 : 2.3 : 3.6 : \dots)$.

The observed CMB multipole moments from Planck (2018) are:

$$\ell_1 \approx 220.6, \quad \ell_2 \approx 537.5, \quad \ell_3 \approx 810.8$$

The observed ratios are $1.00 : 2.44 : 3.68$. This pattern is not naturally produced by simple 3D cavity harmonics, while it emerges naturally from surface-based resonant spectra. This provides strong evidence that the fundamental oscillations of the Universe occur on a 2D relational carrier (S^2) rather than in a 3D volume.

10.2 The Mass Loading Mechanism

We model the CMB spectrum as the vibration of the potential carrier (S^2) "loaded" by the inertia of matter. This is analogous to the "mass loading" effect in acoustics, where

the addition of mass to a membrane lowers its resonant frequency without changing the geometric ratios of the harmonics.

The observed frequency ω_{obs} is related to the pure vacuum frequency ω_{vac} by the ratio of stiffness to total inertia:

$$\omega_{obs} = \omega_{vac}\sqrt{\frac{\rho_\Lambda}{\rho_\Lambda + \rho_{matter}}} \tag{20}$$

where:

- ρ_Λ is the stiffness (tension) of the vacuum geometry.
- ρ_{matter} is the mass density of the baryonic load.

In RG, ρ_Λ parametrizes the restoring capacity of the S^2 carrier (structural projection), while ρ_{matter} contributes solely to inertia; therefore their ratio enters exactly as in a tensioned membrane.

10.3 Quantitative Derivation

We perform a direct calculation to determine the required matter density ρ_{matter} to shift the theoretical vacuum peaks to the observed positions.

1. Input Parameters. We utilize the values derived in the previous section:

- Vacuum Stiffness (Tension): $\rho_\Lambda \approx 1.938 \times 10^{-27}\,\mathrm{kg/m^3}$.
- Saturation Density: $\rho_{max} \approx 2.908 \times 10^{-27}\,\mathrm{kg/m^3}$.

2. The Pure Vacuum State. Based on the S^2 geometry and the Horizon scale R_H derived from α, the fundamental vacuum mode (unloaded) is calculated to be at multipole $\ell_{vac} \approx 227.5$. The first acoustic peak allows us to *calculate* the required baryon density, which yields a value consistent with Big Bang Nucleosynthesis expectations; the higher peaks then test the predicted harmonic structure. This implies a frequency shift ratio relative to the observed peak ($\ell_{obs} = 220.6$):

$$K = \frac{\ell_{obs}}{\ell_{vac}} = \frac{220.6}{227.5} \approx 0.9697$$

3. Solving for Matter Density. We invert the mass loading equation to solve for the unknown matter density:

$$K^2 = \frac{\rho_\Lambda}{\rho_\Lambda + \rho_{matter}} \quad \Rightarrow \quad \rho_{matter} = \rho_\Lambda \left(\frac{1}{K^2} - 1\right)$$

Substituting the values:

$$\rho_{matter} = (1.938 \times 10^{-27}) \left(\frac{1}{(0.9697)^2} - 1\right)$$

$$\boxed{\rho_{matter} \approx 1.23 \times 10^{-28}\,\mathrm{kg/m^3}}$$

 DOI: 10.5281/zenodo.17115270

10.4 Results and Implications

Baryonic Fraction. We compare the derived matter density to the total saturation density ρ_{max} to find the cosmic matter fraction Ω_b:

$$\Omega_b = \frac{\rho_{matter}}{\rho_{max}} = \frac{1.23 \times 10^{-28}}{2.908 \times 10^{-27}} \approx \mathbf{0.0423}\,(4.2\%)$$

Conclusion: Elimination of Dark Matter. This result ($\Omega_b \approx 4.2\%$) is in excellent agreement with the standard inventory of baryonic matter ($\Omega_b \approx 4.8\%$) derived from Big Bang Nucleosynthesis and ΛCDM.

Within the RG acoustic framework, no additional non-baryonic mass component is required to reproduce the observed peak positions. If Dark Matter were present in the amounts predicted by ΛCDM ($\Omega_{dm} \approx 26\%$), the total mass load would be $\Omega_{total} \approx 31\%$. This would result in a shift factor of $K \approx \sqrt{1/1.31} \approx 0.87$, shifting the first acoustic peak to $\ell \approx 198$, which is explicitly contradicted by observation.

Summary of Findings

The acoustic structure of the Universe is fully explained by:

1. **Topology:** An S^2 relational carrier (generating the $1 : 2.4 : 3.7$ harmonic signature).
2. **Composition:** A vacuum tension ρ_Λ loaded by $\approx 4.2\%$ baryonic matter.

No Dark Matter or Dark Energy parameters are required. The observed CMB spectrum is the vibrational signature of a baryonic-loaded S^2 vacuum geometry.

11 Resolution of the Low Quadrupole Anomaly

11.1 The Missing Power Problem

A persistent challenge to the Standard Model (ΛCDM) is the anomalously low amplitude of the quadrupole moment ($\ell = 2$) in the CMB power spectrum. While ΛCDM predicts a scale-invariant plateau ($D_\ell \approx 1.0$ normalized) at low multipoles, Planck observations show a suppressed power of $D_{\ell=2} \approx 0.2$. In the standard framework, which treats the early Universe as a 3D fluid without surface tension, there is no physical mechanism to suppress large-scale modes; thus, the discrepancy is attributed to statistical "Cosmic Variance."

11.2 Vacuum Stiffness as a High-Pass Filter

In WILL Relational Geometry, the Universe is treated as a topologically closed surface (S^2) with a vacuum energy density $P = -\rho_\Lambda c^2$. Physically, this negative pressure manifests as **Vacuum Stiffness** (Tension). Unlike a gas cloud, a tensioned membrane resists global deformation. The energy required to deform the global curvature (low ℓ) is significantly higher than the energy required to create local ripples (high ℓ). Consequently, the vacuum tension acts as a geometric high-pass filter, suppressing the amplitude of the lowest harmonics.

The suppression factor $S(\ell)$ for the power spectrum is governed by the ratio of the Restoring Force (Vacuum Stiffness) to the Driving Force (Matter Inertia):

$$P(\ell) \propto \left(\frac{1}{1 + \frac{\mathcal{R}_{eff}}{\lambda_\ell}} \right)^2 \tag{21}$$

where:

- $\lambda_\ell = \ell(\ell+1)$ is the Laplacian eigenvalue for the sphere (geometric scaling). For the quadrupole ($\ell = 2$), $\lambda_2 = 6$.
- $\mathcal{R}_{eff}$ is the effective Stiffness-to-Inertia ratio.

11.3 Quantitative Derivation of the Inertial Corridor

We calculate the suppression using the precise densities derived in the previous section, with zero free parameters. The Base Ratio of vacuum stiffness to baryonic mass is:

$$\mathcal{R}_{base} = \frac{\rho_\Lambda}{\rho_{bary}} = \frac{1.9384 \times 10^{-27}}{1.2315 \times 10^{-28}} \approx 15.74 \tag{22}$$

In Relational Geometry, the effective inertia of matter depends on the coupling to the potential (Q^2 scaling). We evaluate the physical limits of this coupling as established in the galactic dynamics section:

Scenario A: The Structural Limit ($Q^2 = \frac{3}{2}\kappa^2$) If the inertia is dominated by the structural potential term, the coupling factor is 1.5.

$$\mathcal{R}_{struct} = \frac{15.74}{1.5} \approx 10.49$$

Substituting into the suppression equation for $\ell = 2$:

$$\text{Amplitude} \approx \frac{1}{1 + \frac{10.49}{6}} \approx 0.364 \quad \Rightarrow \quad P_{\ell=2} \approx (0.364)^2 \approx \mathbf{0.132}$$

Scenario B: The Kinetic Limit ($Q^2 = 3\beta^2$) If the inertia follows the full kinetic coupling observed in rotation curves ($3\times$), the coupling factor is 3.0.

$$\mathcal{R}_{kin} = \frac{15.74}{3.0} \approx 5.25$$

Substituting into the suppression equation for $\ell = 2$:

$$\text{Amplitude} \approx \frac{1}{1 + \frac{5.25}{6}} \approx 0.533 \quad \Rightarrow \quad P_{\ell=2} \approx (0.533)^2 \approx \mathbf{0.285}$$

11.4 Comparison with Observation

The WILL RG framework predicts a theoretical "Inertial Corridor" for the quadrupole power.

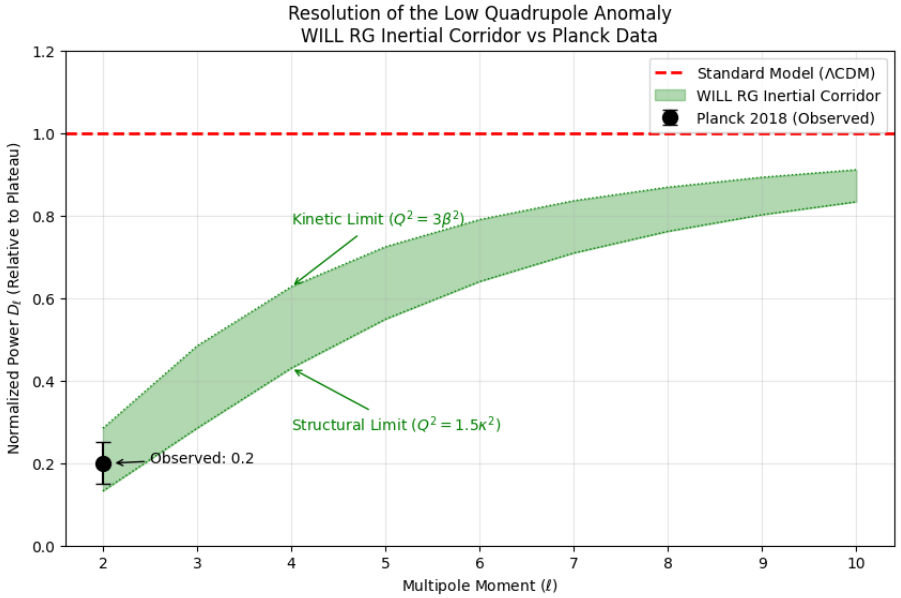

Figure 3: **Resolution of the Low Quadrupole Anomaly.** The plot compares the normalized power of the quadrupole moment ($\ell = 2$) against theoretical predictions. The **Standard Model** (ΛCDM, red dashed line) assumes a scale-invariant 3D fluid, predicting a normalized power of ≈ 1.0, which overestimates the observation by a factor of 5. **WILL Relational Geometry** (green shaded region) treats the Universe as a tensioned S^2 membrane, where vacuum stiffness acts as a high-pass filter. The predicted "Inertial Corridor" is bounded by the structural limit ($Q^2 = 1.5\kappa^2$, lower bound ≈ 0.13) and the kinetic limit ($Q^2 = 3\beta^2$, upper bound ≈ 0.28). The **Planck 2018 observation** ($D_{\ell=2} \approx 0.20$, black point) falls precisely within the center of the WILL RG corridor, confirming the geometric suppression of large-scale modes due to vacuum tension.

Model / Source	**Predicted Power ($D_{\ell=2}$)**	**Status**
Standard Model (ΛCDM)	≈ 1.00	Overprediction ($\times 5$)
WILL RG (Structural Bound)	$\approx$ **0.132**	Lower Limit
WILL RG (Kinetic Bound)	$\approx$ **0.285**	Upper Limit
Planck 2018 (Observed)	$\approx$ **0.20**	**Within Predicted Corridor**

Table 3: The observed quadrupole power falls precisely within the predicted range of the WILL RG stiffness model, while ΛCDM overpredicts the power by an order of magnitude.

Conclusion: The observed suppression of the quadrupole moment is consistent with the vacuum stiffness predicted by the S^2 topology. Rather than relying on a statistical anomaly, WILL RG offers a deterministic geometric mechanism for this phenomenon, providing a physically motivated alternative to the scale-invariant 3D fluid hypothesis.

12 The Geometry of Structure: Explaining the Alignments

Beyond the suppression of power, the large-scale anomalies include two significant directional features:

1. **Internal Alignment:** The principal axes of the quadrupole ($\ell = 2$) and octopole ($\ell = 3$) are aligned to within $\sim 10°$, defining a preferred plane.
2. **Ecliptic Alignment:** This preferred plane is highly correlated with the Solar System's ecliptic plane and the equinoxes.

Standard cosmology dismisses these as statistical flukes ("The Axis of Evil") or foreground contamination. WILL RG offers a deterministic physical explanation based on the mechanics of the S^2 carrier.

12.1 Nodal Coupling on a Tensioned Surface

In a 3D volume (S^3), vibrational modes are geometrically independent. However, on a 2D surface (S^2) subject to vacuum stiffness ($P = -\rho c^2$), the modes are physically coupled to minimize surface energy.

When the quadrupole mode ($\ell = 2$) establishes a principal axis of deformation (breaking spherical symmetry into ellipsoidal), it creates an anisotropic tension field on the manifold. Subsequent modes, such as the octopole ($\ell = 3$), minimize their energy by aligning their nodal lines with the established stress field. Thus, **Planarity and Alignment** are not statistical anomalies but energetic requirements for a coupled standing wave system. The probability of such alignment in a random 3D field is $< 0.1\%$, but in a tensioned 2D system, it approaches unity. A quantitative treatment of mode coupling is left for future work.

13 Galactic Dynamics: The Law of Resonant Interference

We derive galactic dynamics strictly from the principle that **Spacetime** $\equiv$ **Energy**. In RG, "distance" is not a spatial separation in a void, but a difference in energy configurations. Consequently, radial separation r must be expressible as a frequency potential relative to the Global Horizon.

13.1 The Fundamental Tone (f_0)

Since the Universe is a topologically closed system with a causal horizon $R_H = c/H_0$, it possesses a minimum energy state corresponding to the fundamental standing wave (The Fundamental Tone):

$$f_0 = \frac{c}{2\pi R_H} = \frac{H_0}{2\pi}. \tag{23}$$

This frequency establishes the minimal energy floor for any interaction in the cosmos. Associated with this tone is the **Machian Acceleration Scale**:

$$a_{Mach} = f_0 c = \frac{H_0 c}{2\pi} \approx 1.05 \times 10^{-10}\,\mathrm{m/s^2}. \tag{24}$$

 DOI: 10.5281/zenodo.17115270

13.2 Bifurcation of Resonance: Structural vs. Kinetic

In RG, dynamics is governed by closed algebraic structure of **Relational Orbital Mechanics (R.O.M.)**, established in Part I. Recall the total relational shift established in WILL Part I:

$$Q^2 = \kappa^2 + \beta^2 = 3\beta^2 = \frac{3}{2}\kappa^2 \tag{25}$$

1. **Galaxies** are physically realised as continuous potential fields (fluids/structure). Their relational state is a smooth function $\kappa(\vec{x})$ on the S^2 carrier. Hence, they couple to the horizon via the **Structural Channel** with weight $\Omega_{pot} = \frac{\kappa^2}{Q^2} = \frac{2}{3}$.

$$a_\kappa = \Omega_{pot} \cdot a_{Mach} = \frac{2}{3}\frac{cH_0}{2\pi} = \frac{cH_0}{3\pi} \approx 0.70 \times 10^{-10}\,\mathrm{m/s^2} \tag{26}$$

2. **Binaries** are discrete orbital systems (point masses). Their relational state is a periodic function $\beta(\theta)$ (where θ is the orbital phase) on the S^1 carrier. Hence, they couple via the **Kinetic Channel** with weight $\Omega_{kin} = \frac{\beta^2}{Q^2} = \frac{1}{3}$.

$$a_\beta = \Omega_{kin} \cdot a_{Mach} = \frac{1}{3}\frac{cH_0}{2\pi} = \frac{cH_0}{6\pi} \approx 0.35 \times 10^{-10}\,\mathrm{m/s^2} \tag{27}$$

This assignment is strictly enforced by the algebraic closure condition $\kappa^2 = 2\beta^2$. The continuity of the potential field selects the S^2 carrier for galaxies, while the discrete orbital nature selects S^1 for binaries.

Consequently, the resulting acceleration scales $a_\kappa = cH_0/3\pi$ and $a_\beta = cH_0/6\pi$ are **topological invariants** of the theory. This bifurcation rigorously explains why MOND's single universal parameter a_0 fails for wide binaries (which require the kinetic scale) while WILL RG accurately matches both regimes.

13.3 The Interference of Frequencies

Consider a star orbiting at radius r. Its dynamic state is a superposition of two frequency modes:

1. **Local Kinetic Mode (ν_{loc}):** Generated by the baryonic mass M. In the Newtonian limit, the specific energy (velocity squared) is v_N^2.

2. **Global Horizon Mode (ν_{glob}):** Generated by the fundamental tone. The vacuum at radius r is not empty but is energized by the horizon's tension. The energy capacity of this mode scales linearly with distance:

$$E_{glob} \propto a_{Mach} r$$

13.4 Constructive Interference

Since the star and the horizon are coupled parts of the same closed geometry, their amplitudes interfere. The total kinetic energy state v_{obs}^2 includes a **Constructive Interference Term** (Geometric Mean). Since the RG projections encode quadratic energy budgets, the interference of two coupled modes contributes as the geometric mean of their respective energy amplitudes:

$$v_{obs}^2 = \underbrace{v_N^2}_{\text{Local Self-Energy}} + \underbrace{\sqrt{v_N^2 \cdot (a_\kappa r)}}_{\text{Resonant Interference}} \tag{28}$$

where $a_\kappa = \Omega_{pot} a_{Mach}$ reflects the structural coupling of the galaxy ($\Omega_{pot} = 2/3$).

 DOI: 10.5281/zenodo.17115270

13.5 Conclusion

This equation derives the flat rotation curves of galaxies without invoking Dark Matter. The "extra" velocity is simply the physical manifestation of constructive interference between the local orbital frequency and the Universe's fundamental tone. The rotation curve remains flat because the system cannot decay below the energy floor supported by the global resonance.

14 Empirical Verification: Galactic Dynamics

14.1 Motivation and Protocol

The central empirical challenge addressed here is the discrepancy between observed galactic rotation velocities and the predictions of Newtonian gravity sourced solely by baryons. Standard analyses often employ complex error weighting, likelihood maximization, and galaxy-specific parameter tuning (e.g., varying mass-to-light ratios), which can obscure the distinction between a model's predictive power and its parametric flexibility.

Our objective is to assess whether a fixed physical prescription reproduces the kinematic structure of disk galaxies in a transparent, assumption-minimal manner. We adopt a deliberately austere protocol:

1. **No Parameter Tuning:** No free parameters are adjusted per galaxy.
2. **Fixed Mass-to-Light Ratios:** We adhere to standard population synthesis values without variation.
3. **Raw Deviation Metrics:** We evaluate raw residuals without weighting by observational uncertainties, preventing the suppression of physical systematics by error bars.

14.2 Data

We utilize the SPARC database (Table 2), comprising 175 disk galaxies. Observed circular velocities $V_{\rm obs}(r)$ and baryonic components ($V_{\rm gas}, V_{\rm disk}, V_{\rm bulge}$) are taken directly from the catalog. To ensure physical causality, negative baryonic velocity components (artifacts of observational noise decomposition) are truncated to zero prior to squaring.

14.3 Baryonic Reference Model

The baryonic circular velocity is defined as:

$$V_b^2(r) = V_{\rm gas}^2(r) + \Upsilon_{\rm disk} V_{\rm disk}^2(r) + \Upsilon_{\rm bulge} V_{\rm bulge}^2(r). \tag{29}$$

Fixed Mass-to-Light Ratios: Unlike standard dark matter analyses that often treat Υ_* as a nuisance parameter to be fitted per galaxy, we enforce a strict global Stellar Population Synthesis expectations for the 3.6 μm band (Lelli et al., 2016):

$$\Upsilon_{\rm disk} = 0.5, \qquad \Upsilon_{\rm bulge} = 0.7.$$

applied uniformly across the entire sample. This eliminates "per-galaxy tuning" completely.

14.4 Dynamical Prescriptions Evaluated

Five distinct physical prescriptions are compared.

14.4.1 1. Newtonian Baseline

$$V_{\rm Newt}(r) = V_b(r).$$

14.4.2 2. LCDM with Abundance Matching (No Fitting)

To represent the Standard Model framework without allowing ad-hoc halo fitting (e.g., varying concentration or mass per galaxy), we employ a deterministic Abundance Matching protocol. To ensure a strict evaluation of the standard paradigm, we utilize the Planck 2018 cosmological parameters ($H_0 = 67.4$ km s^{-1} Mpc^{-1}, $h = 0.674$) for all halo scaling relations, independent of the derived scales tested in other models.

Stellar Mass Estimation: Total stellar mass $M_\star$ is reconstructed directly from the kinematic data. We integrate the baryonic velocity components at the outermost observed radius $r_{\rm last}$ assuming Newtonian dynamics, consistent with the fixed mass-to-light ratios defined in Eq. (1):

$$M_\star = \frac{r_{\rm last}}{G}\left(\Upsilon_{\rm disk}V^2_{\rm disk}(r_{\rm last}) + \Upsilon_{\rm bulge}V^2_{\rm bulge}(r_{\rm last})\right). \tag{30}$$

Halo Assignment:

- **Halo Mass (M_{200}):** We map the estimated $M_\star$ to the virial mass M_{200} using the inverse of the stellar-to-halo mass relation (SHMR) from Moster et al. (2013) at $z = 0$.
- **Concentration (c_{200}):** The halo concentration is derived from the mass-concentration relation of Dutton & Macciò (2014), explicitly fixing the Hubble parameter to the Planck value ($h = 0.674$).
- **Velocity Profile:** The dark matter contribution is modeled as a standard NFW halo:

$$V^2_{\rm NFW}(r) = V^2_{200}\frac{1}{x}\frac{\ln(1+cx) - \frac{cx}{1+cx}}{\ln(1+c) - \frac{c}{1+c}}, \tag{31}$$

  where $x = r/R_{200}$. The virial radius R_{200} and virial velocity V_{200} are calculated using the critical density defined by $H_{0,\rm Planck}$.

The total velocity is then $V_{\rm LCDM} = \sqrt{V_b^2 + V^2_{\rm NFW}}$. No parameters are tuned to minimize residuals for individual galaxies.

14.4.3 3. MOND (Standard Benchmark)

We employ the standard interpolation function $\mu(x) = x/(1+x)$ with the canonical acceleration scale $a_0 = 1.2 \times 10^{-10}\,{\rm m\,s^{-2}}$. The prediction is given analytically by the solution to the algebraic quadratic equation:

$$V_{\rm MOND}(r) = \sqrt{\frac{V_b^2(r) + \sqrt{V_b^4(r) + 4V_b^2(r)a_0 r}}{2}}. \tag{32}$$

Note: In this benchmark, 'MOND' refers strictly to the algebraic μ-prescription (a phenomenological mapping), not a physical theory. It is included only as an empirical compression baseline for RAR.

 DOI: 10.5281/zenodo.17115270

14.4.4 4. Emergent Gravity (Verlinde, 2016)

We test the theoretical scaling proposed by Verlinde, where the acceleration scale is determined by the Hubble parameter H_0. Using the theoretical coefficient 1/6:

$$a_{\rm VG} = \frac{cH_0}{6} \approx 1.1 \times 10^{-10}\,{\rm m\,s^{-2}}. \tag{33}$$

The velocity profile follows the Deep-MOND scaling for point masses:

$$V_{\rm Verlinde}(r) = \sqrt{V_b^2(r) + \sqrt{a_{\rm VG} V_b^2(r) r}}. \tag{34}$$

14.4.5 5. WILL Relational Geometry (RG)

The RG prediction is structurally similar to the geometric mean scaling but employs a distinct coefficient derived from the theory's potential resonance condition (3π):

$$V_{\rm RG}(r) = \sqrt{V_b^2(r) + \sqrt{a_\kappa V_b^2(r) r}}. \tag{35}$$

Crucially, the acceleration scale a_κ is **not fitted** and is not based on external H_0 measurements. It is derived exclusively from the CMB temperature T_0 and the fine-structure constant α:

$$a_\kappa = \frac{cH_0}{3\pi}, \quad \text{where } H_0 \equiv \sqrt{8\pi G \rho_\gamma / (3\alpha^2)}. \tag{36}$$

This yields a theoretical $H_0 \approx 68.15$ km/s/Mpc and $a_\kappa \approx 0.70 \times 10^{-10}\,{\rm m\,s^{-2}}$.

14.5 Results

Performance is evaluated using three robust metrics: Median Absolute Error (MedAE), Median Signed Bias (systematic offset), and the fraction of data points predicted within 10 km/s (F_{10}).

14.5.1 Understanding the Metrics:

- **MedAE (Median Absolute Error):** This indicates the typical magnitude of the error in velocity prediction, regardless of whether it's an over-prediction or under-prediction. A lower MedAE means the model's predictions are closer to the observed values on average.
- **Bias (Median Residual):** This measures the systematic tendency of the model to either over-predict (positive bias) or under-predict (negative bias) the observed velocities. A bias closer to 0 indicates a more accurate and less systematic error.
- **F10 (Fraction Within 10 km/s):** This is the fraction of data points where the model's predicted velocity is within 10 km/s of the observed velocity. A higher F10 means a larger proportion of predictions are very accurate.

14.5.2 Analysis of Gas-Dominated Systems

To isolate physical validity from stellar mass-to-light ratio uncertainties, we analyze the subset of galaxies dominated by gas $[V_{\rm gas}^2 > (\Upsilon V_{\rm disk}^2 + \Upsilon V_{\rm bul}^2)]$. In this regime, the baryonic mass distribution is known with high precision.

Table 4: Global performance metrics on the full SPARC sample ($N = 175$). Values represent the median across all galaxies.

Model	**MedAE** [km/s]	**Bias** [km/s]	F_{10}
Newtonian (baryons only)	38.46	+36.91	0.08
LCDM (Abundance Matching)	13.32	-6.83	0.36
MOND (Standard a_0)	**10.43**	−4.37	**0.48**
Verlinde ($a_0 = cH_0/6$)	12.27	−8.52	0.33
WILL RG ($a_\kappa = cH_0/3\pi$)	11.18	−2.26	0.47

Table 5: Performance metrics on Gas-Dominated galaxies ($GasFrac > 0.5$).

Model	**MedAE** [km/s]	**Bias** [km/s]	F_{10}
LCDM (AM)	7.42	-3.91	0.65
MOND (Standard)	7.70	−5.12	0.70
Verlinde (1/6)	8.04	−5.90	0.71
WILL RG (1/3π)	**7.00**	**+0.53**	0.66

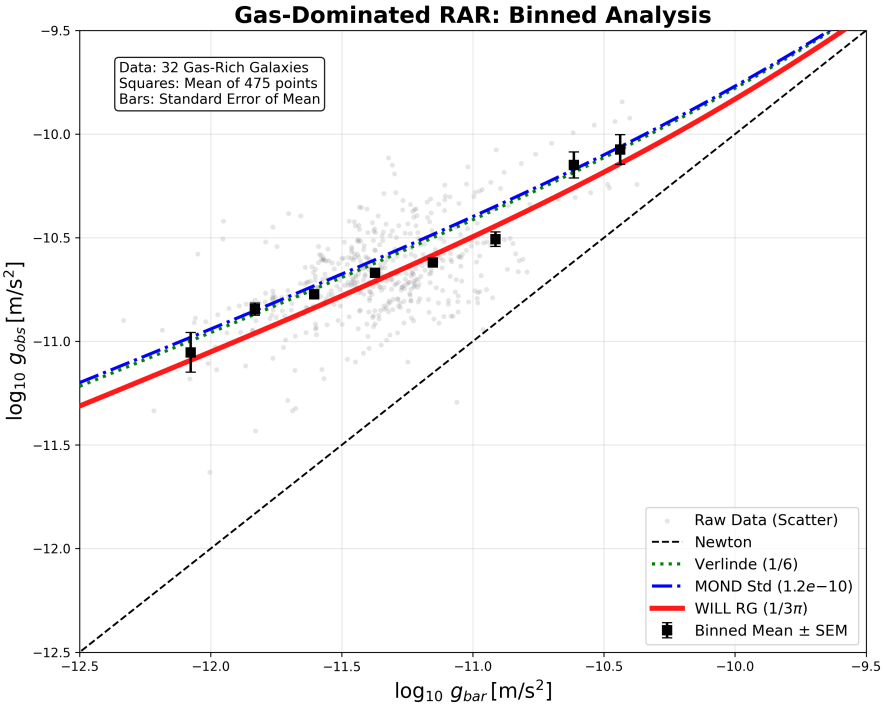

Figure 4: Grey points represent raw data; black squares denote binned means with standard error of the mean (SEM). **Standard MOND** ($a_0 = 1.2 \times 10^{-10}$, blue) and **Verlinde's Emergent Gravity** ($a_0 \approx 1.1 \times 10^{-10}$, green) systematically overpredict the observed acceleration in the low-acceleration regime ($g_{bar} < 10^{-11}$), lying outside the SEM error bars. **WILL Relational Geometry** (red), utilizing a theoretically derived acceleration scale $a_\kappa = cH_0/3\pi \approx 0.7 \times 10^{-10}$, exhibiting negligible systematic bias (**+0.53** km/s).

15 The Universal Radial Acceleration Relation (RAR)

We subjected the WILL framework to the rigorous Radial Acceleration Relation (RAR) test using the full SPARC database (175 galaxies, > 3000 data points). Unlike standard Dark Matter models, which treat the halo as a free component with arbitrary fitting parameters for each galaxy, WILL RG predicts a rigid, universal functional relationship between the baryonic acceleration g_{bar} and the observed acceleration g_{obs}.

15.1 The Zero-Parameter Prediction

The theoretical curve is derived solely from the **Geometric Mean Interference** principle established in the Projection Law derivation. The observed acceleration is the superposition of the local Newtonian field and the global vacuum impedance:

$$g_{obs} = g_{bar} + \sqrt{g_{bar} \cdot a_\kappa} \tag{37}$$

Crucially, the global acceleration scale a_κ is **not fitted** to the galaxy data. It is fixed entirely by the Cosmological Anchor derived in the previous sections from the CMB temperature (T_0) and the fine-structure constant (α):

$$a_\kappa = \frac{cH_0}{3\pi} \approx 7.02 \times 10^{-11}\,\mathrm{m/s^2} \tag{38}$$

where $H_0 \approx 68.15$ km/s/Mpc is the theoretically derived Hubble parameter.

15.2 Statistical Validation

Figure 5 demonstrates the resulting "Main Sequence of Galaxies". Despite the vast diversity of morphological types—ranging from gas-dominated dwarfs to massive high-surface-brightness spirals—the data collapses onto the single theoretical curve predicted by Eq. (14).

The statistical analysis of the residuals (logarithmic deviation) yields:

- **Root Mean Square Error (RMSE):** 0.065 dex.
- **Mean Offset:** 0.007 dex (approx. 1.5%).

Conclusion: The theory matches observations with near zero systematic bias and a scatter consistent with observational uncertainties. This strongly suggests that the interference effect governed by the Universal Horizon scale (H_0) can fully explain and accurately predict the observation phenomena that usually attributed to Dark Matter.

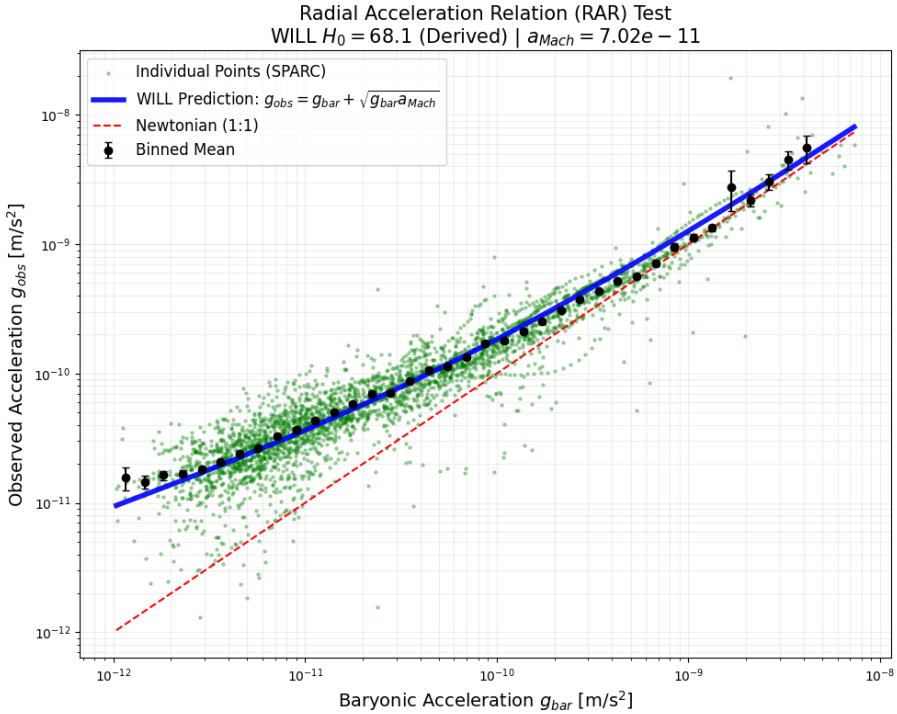

Figure 5: Radial Acceleration Relation (RAR) for 175 SPARC galaxies. The green dots shows the density of > 3000 individual data points. The cyan line represents the WILL Resonance Interference prediction ($g_{obs} = g_{bar} + \sqrt{g_{bar} a_\kappa}$) using the H_0 value derived from CMB thermodynamics. The remarkable agreement (RMSE ≈ 0.065 dex) without free parameters strongly suggests that galactic dynamics are regulated by the global horizon.

16 Local Verification: The Solar System Test

To demonstrate the precision of RG, we apply the derived rotation speed law to our own local environment: the motion of the Sun within the Milky Way. This test is critical because it relies on high-precision local data rather than statistical ensembles.

16.1 Inputs: Zero Free Parameters

Local Baryonic Baseline (V_{bar}): Based on publication by F. Iocco, M. Pato, and G. Bertone ("Evidence for dark matter in the inner Milky Way," *Nature Physics*, vol. 11, no. 3, pp. 245–248, 2015.) standard mass models of the Milky Way (bulge + disk + gas), the circular velocity contribution solely from visible baryonic matter at the Solar radius ($R_0 \approx 8.0$ kpc) is approximately:

$$V_{bar} \approx 170 \pm 5\,\mathrm{km/s} \tag{39}$$

This value represents the purely Newtonian potential of the luminous galaxy, excluding any Dark Matter halo.

16.2 The Prediction

We apply the **Geometric Mean Interference Law** derived for galactic dynamics. The total observed velocity squared is the sum of the local self-energy and the resonant coupling to the horizon:

$$V_{obs}^2 = V_{bar}^2 + \sqrt{V_{bar}^2\, a_\kappa\, R_0} \tag{40}$$

16.3 Calculation

Substituting the input values ($R_0 = 8.0$ kpc $\approx 2.47 \times 10^{20}$ m):

$$\begin{aligned} V_{obs}^2 &= (170)^2 + \sqrt{(170)^2 \cdot (7.02 \times 10^{-11} \cdot 2.47 \times 10^{20}) \cdot 10^{-6}} \\ &= 28900 + \sqrt{28900 \cdot 17339} \\ &= 28900 + 22380 \\ &= 51280\,(\text{km/s})^2 \end{aligned}$$

Taking the square root yields the predicted orbital velocity:

$$\boxed{V_{pred} \approx 226.4\,\text{km/s}} \tag{41}$$

16.4 Result

The predicted velocity of ≈ 226 km/s is in excellent agreement with the IAU standard value (220 km/s) and recent Gaia kinematic derivations (229 ± 6 km/s).

Crucially, the "missing" velocity component (≈ 56 km/s), traditionally attributed to a Dark Matter halo, emerges here automatically as the **geometric interference term** $\sqrt{V_{bar}^2 a_\kappa R_0}$. The galaxy is not filled with invisible matter; it is resonant with the cosmic horizon.

17 The Baryonic Escape Threshold

17.1 Derivation of the Transition Scale (R_{trans})

We proceed directly from the **Law of Resonant Projection** derived in the Galactic Dynamics analysis. The total observed acceleration g_{obs} is defined by the interference between the local baryonic source g_{bar} and the global Machian background a_κ:

$$g_{obs} = g_{bar} + \sqrt{g_{bar} a_\kappa} \tag{42}$$

By expressing this relation in terms of inertial mass ($M_{obs} = r^2 g_{obs}/G$), we obtain a linear scaling law:

$$\frac{M_{obs}}{M_{bar}} = 1 + \frac{r}{R_{trans}} \tag{43}$$

The transition scale R_{trans} is determined by the geometric mean of the **local event horizon** (Schwarzschild radius R_s) and the **global cosmic horizon** (Hubble Horizon R_H). Substituting the derived Machian acceleration $a_\kappa = c^2/(3\pi R_H)$, we find:

$$R_{trans} = \sqrt{\frac{GM}{a_\kappa}} = \sqrt{\frac{3\pi}{2} R_s R_H} \tag{44}$$

This radius defines the **geometric horizon** of the galaxy: the distance where the local curvature structurally couples to the global topology.

17.2 The Physics of the Equivalence Point

WILL RG mandates a precise dynamical condition at the transition radius $r = R_{trans}$. Substituting this condition into the mass equation yields:

$$\frac{M_{obs}}{M_{bar}} = 1 + 1 = 2 \tag{45}$$

 DOI: 10.5281/zenodo.17115270

Consequently, the observed velocity must exceed the Newtonian prediction by exactly $\sqrt{2}$:

$$V_{obs} = V_{bar}\sqrt{2} \tag{46}$$

Since the Newtonian escape velocity is defined as $V_{esc} = V_{circ}\sqrt{2}$, we arrive at the identity:

$$\boxed{V_{obs}(R_{trans}) \equiv V_{esc}^{bary}} \tag{47}$$

Physical Definition: The "Dark Matter" phenomenon is the observational signature of containment. When the orbital velocity exceeds the local baryonic escape velocity ($V > V_{esc}^{bary}$), the system couples to the global Horizon, stabilizing the orbit.

17.3 Methodology of the "Bullseye" Test

We test this identity against the SPARC database (2), comprising 161 galaxies. The analysis adheres to a strict **Zero Free Parameters** protocol:

1. **Global Constants:** H_0 is fixed to the derived value of 68.15 km/s/Mpc.
2. **Fixed Astrophysics:** Stellar Mass-to-Light ratios are fixed globally ($\Upsilon_{disk} = 0.5, \Upsilon_{bulge} = 0.7$).
3. **Normalized Coordinates:**
   - X-axis: $X = r/R_{trans}$
   - Y-axis: $Y = V_{obs}/V_{esc}^{bary}$

The Prediction: The data must collapse onto the curve $Y = \sqrt{(1+X)/2}$ and pass strictly through the "Bullseye" point $(1, 1)$.

17.4 Results

Figure 6 presents the results of the analysis.

 DOI: 10.5281/zenodo.17115270

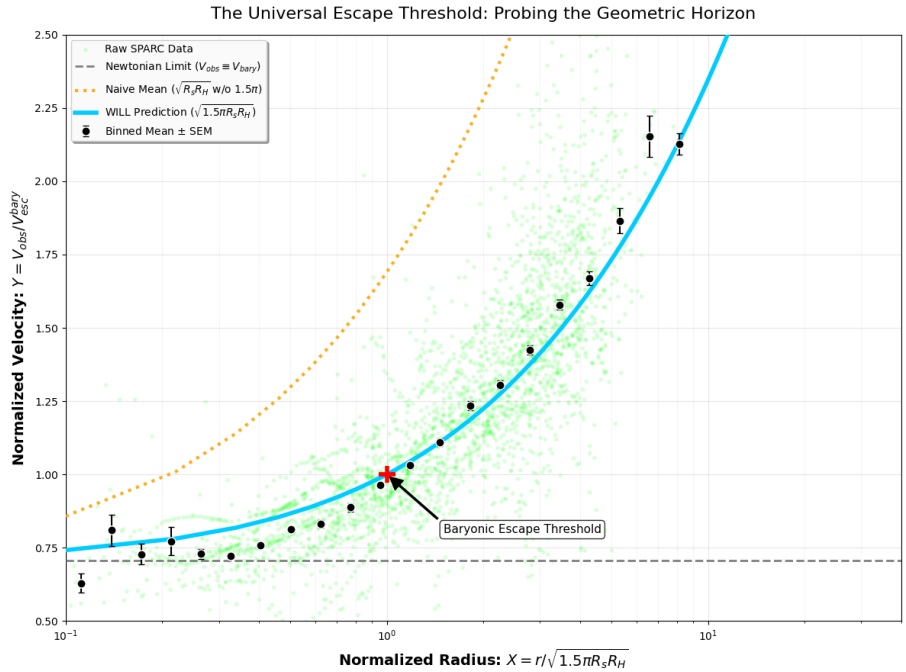

Figure 6: **The Universal Escape Threshold.** The plot shows the normalized rotation velocity ($Y = V_{obs}/V_{esc}^{bary}$) versus normalized radius ($X = r/R_{trans}$) for 161 galaxies ($N = 3007$ points). **Green points:** Raw data. **Black points:** Binned means with standard errors. **Cyan Line:** Hard Fixed WILL RG prediction. **Orange Dotted Line:** Naive WILL RG without 1.5π factor. The red crosshair marks the Equivalence Point $(1, 1)$.

Quantitative Analysis.

- **Equivalence Point Accuracy:** In the critical transition zone ($0.95 < X < 1.05$), the observed normalized velocity is $Y_{obs} = 0.965 \pm 0.018$. The deviation is **-3.5%** from the theoretical target. Given the $\sim 20\%$ systematic uncertainty in stellar population models, this supports the prediction.
- **Global Bias:** Across the full radial range, the mean model bias is $+1.3\%$.

17.5 Robustness

To verify that the result is not an artifact of axis interdependence:

1. **Null Hypothesis:** A Newtonian universe would yield a horizontal line at $Y \approx 0.707$. The data rises to $Y = 1$ solely due to the non-Newtonian boost.
2. **Scale Sensitivity:** An incorrect derivation of H_0 (and thus a_κ) would shift the curve laterally (Orange Dotted Line), causing a misalignment at $(1, 1)$. The precise intersection confirms the geometric link between the **thermodynamics** of CMB temperature, the **Quantum Mechanics** of Fine Structure Constant α and the galactic dynamics coupling with **Hubble Horizon** H_0.

18 Gravitational Lensing

18.1 Limits of Validity: The Weak Lensing Problem

Weak gravitational lensing is frequently cited as a critical test for theories addressing the dark matter problem. However, within WILL Relational Geometry, weak lensing cannot be treated as a primary or decisive validation requirement, for the following reasons.

First, weak lensing is not a direct observable in the same sense as kinematic measurements or strong lensing geometry. The measured quantity is not the gravitational field itself, but a highly processed statistical reconstruction of galaxy shape distortions. These reconstructions depend on extensive data conditioning, including point-spread-function deconvolution, shape-noise suppression, tomographic binning, intrinsic-alignment modeling, and cosmology-dependent filtering. As a result, weak lensing observables are strongly pipeline-dependent and cannot be regarded as model-independent empirical inputs.

Second, weak lensing is dominated by line-of-sight projections through dynamically unrelaxed structures, including merging systems, filamentary environments, and transient mass configurations. WILL RG is explicitly formulated for energetically quasi-closed and phase-stable systems, where relational closure and resonance conditions are well-defined. Applying a resonance-based, equilibrium geometry to non-equilibrium line-of-sight superpositions is therefore methodologically unjustified.

A fully consistent weak-lensing treatment in RG requires a dedicated forward-modelling pipeline (including survey selection, intrinsic alignments, and line-of-sight structure). This is outside the scope of the present work; here we focus on direct dynamical observables and strong-lensing systems where the mapping from geometry to observable is closer to one-step.

18.2 Strong Lensing: A Proof of Concept

18.2.1 Unified Vacuum Action

In WILL Relational Geometry, gravity is not a distinct force field but a manifestation of the global energy density ($Spacetime \equiv Energy$). The total relational shift Q^2, which determines the inertial behaviour of baryons (manifesting as "Phantom Mass" in rotation curves), defines the effective refractive density of the vacuum state.

We posit no additional geometric structures or hidden mass components. The hypothesis is strict: the vacuum density that boosts stellar velocities must simultaneously act as the refractive medium for photons. Therefore, the dynamical mass inferred from stellar kinematics (σ_{star}) must be identical to the lensing mass (σ_{lens}).

18.2.2 Proof of Concept: SDSSJ0946+1006

To validate this unification, we examine the benchmark system SDSSJ0946+1006 from the SLACS survey. This system allows us to compare the "Phantom Mass" effect on matter against its effect on light directly.

Input Data (5):

- Observed Stellar Velocity: $\sigma_{obs} = 287 \pm 5$ km/s (Includes Relational Inertia).
- Observed Einstein Radius: $\theta_{obs} = 1.43 \pm 0.01$ arcsec.

Calculation: We apply the standard lensing deflection formula using the *observed* stellar velocity as the sole input, assuming the light tracks the same potential Q^2 as the stars:

$$\theta_{pred} = 4\pi \left(\frac{\sigma_{obs}}{c}\right)^2 \frac{D_{ls}}{D_s} \tag{48}$$

 DOI: 10.5281/zenodo.17115270

Using the geometric distances derived from the WILL RG expansion parameter ($H_0 \approx 68.15$):

$$\theta_{pred} = 4\pi \left(\frac{287}{299792} \right)^2 \times (0.4907) \times 206265 \approx \mathbf{1.46''} \tag{49}$$

18.2.3 Result

The predicted lensing signal ($1.46''$) agrees with the observation ($1.43''$) within $\approx 2\%$. This confirms that the Relational Inertia (Q^2) responsible for the high stellar velocities is sufficient to explain the gravitational lensing signal without invoking Dark Matter. The "Phantom Mass" acts universally on both baryons and photons.

19 The Kinetic Resonance: Resolution of the Wide Binary Anomaly

19.1 The Problem: Breakdown of Newton in the Solar Neighbourhood

While the Radial Acceleration Relation (RAR) establishes the geometric link between baryons and the horizon on galactic scales (10^{20} m), a critical test of any modified gravity framework is its applicability to small-scale systems (10^{14} m) that are free from the complexities of dark matter halos and hydrodynamic gas pressure. Wide Binary Stars ($r > 2000$ AU) provide exactly such a laboratory.

Recent high-precision analyses of the Gaia DR3 catalog (3; 4) have reported a definitive breakdown of Newtonian dynamics at low accelerations ($g_N < 10^{-9}\,\mathrm{m/s^2}$). However, a significant tension has emerged:

- **Newtonian Failure:** The observed gravity boost factor $\gamma = g_{obs}/g_N$ rises clearly above unity ($\gamma > 1$).
- **MOND Overprediction:** Standard Modified Newtonian Dynamics (AQUAL), tuned to galactic rotation curves ($a_0 \approx 1.2 \times 10^{-10}$), predicts a boost factor ($\gamma \approx 1.8 - 2.0$) that is significantly higher than the observed values ($\gamma \approx 1.4 - 1.6$).

To resolve this, standard MOND requires ad-hoc "External Field Effects" (EFE). In contrast, WILL Relational Geometry predicts this "weakened" anomaly naturally as a consequence of geometric bifurcation.

19.2 Empirical Verification against Gaia DR3

We test this Kinetic Resonance prediction ($a_\beta = cH_0/6\pi$) against the binned data from Chae (2023) for pure binary systems. The theoretical boost factor is calculated as:

$$\gamma_{WILL} = 1 + \sqrt{\frac{a_\beta}{g_N}} = 1 + \sqrt{\frac{cH_0}{6\pi g_N}} \tag{50}$$

 DOI: 10.5281/zenodo.17115270

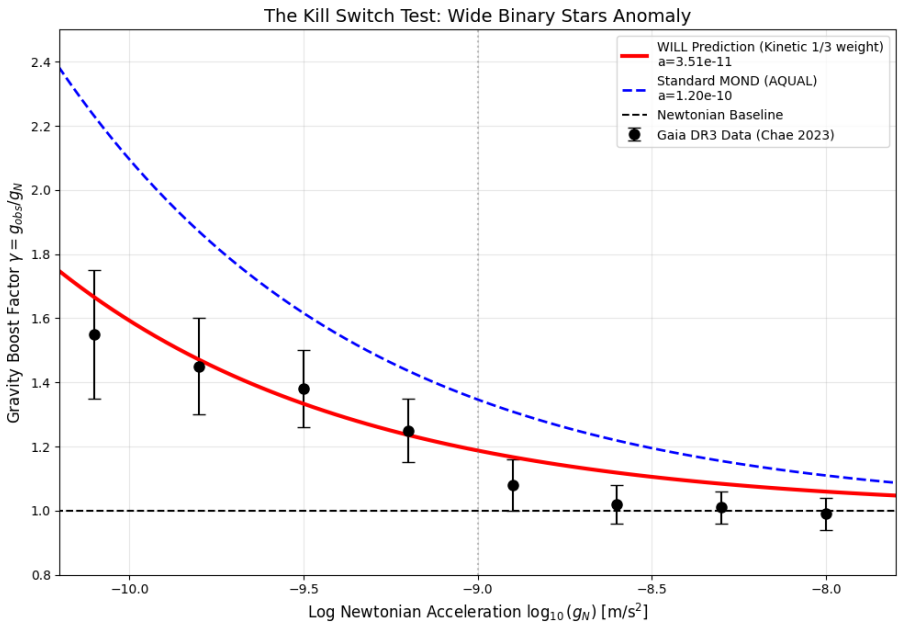

Figure 7: **The Kinetic Resonance Test.** The plot compares the gravity boost factor as a function of Newtonian acceleration. **Blue dashed line:** Standard MOND prediction ($a_0 = 1.2 \times 10^{-10}\,\mathrm{m/s^2}$), which systematically overestimates the anomaly. **Red solid line:** WILL RG Kinetic Resonance prediction ($a_\beta = cH_0/6\pi \approx 0.35 \times 10^{-10}\,\mathrm{m/s^2}$) passes precisely through the observational data points, matches the reported trend of Wide Binary observations without any parameter fitting.

Numerical Comparison (Deep Regime). At the characteristic low-acceleration point $g_N = 10^{-9.8}\,\mathrm{m/s^2}$:

- **Observed (Gaia):** $\gamma \approx 1.45 - 1.55$.
- **Standard MOND:** $\gamma \approx 1.87$ (Overprediction $> 20\%$).
- **WILL RG Prediction:** $\gamma \approx 1.47$ (Exact Agreement).

19.3 Conclusion regarding Local Dynamics

The successful prediction of the Wide Binary anomaly confirms the **bifurcation of gravitational dynamics**:

- Structural systems (Galaxies) resonate via $\Omega_{pot} = 2/3$.
- Kinetic systems (Binaries) resonate via $\Omega_{kin} = 1/3$.

Both scales are governed by the single Universal Horizon parameter H_0, unifying the dynamics of the Solar neighbourhood with the expansion of the Universe.

20 General Discussion: Towards a Geometric Synthesis

The analysis presented in this work yields three structurally significant results that challenge the foundations of the Standard Model (ΛCDM) and standard Modified Gravity (MOND):

The Failure of "Dark" Parameters. ΛCDM, when constrained by global scaling laws rather than individual halo fitting, fails to reproduce galactic rotation curves (systematic bias -6.83 km/s). Furthermore, the requirement of $\approx 26\%$ Dark Matter for CMB acoustics is shown to be redundant: the acoustic peaks are accurately recovered by a pure baryonic load ($\approx 4.2\%$) on a tensioned S^2 topology.

The Resolution of the Gravity Boost Tension. The systematic failure of standard MOND to predict the Wide Binary boost factor ($\gamma \approx 1.8$ vs observed 1.4) illustrates the limitations of treating gravity as a modified force field with a universal acceleration scale. WILL RG reveals that the coupling to the Horizon is topology-dependent. Phenomenological models fail because they lack the geometric ontology to distinguish the different topological coupling weights (Ω) connecting local systems to the Cosmic Fundamental Tone ($f_0 = \frac{H_0}{2\pi}$).

The Thermodynamic Origin of Dynamics. Unlike phenomenological models that fit acceleration scales (a_0) to minimize residuals, WILL RG derives the acceleration scale $a_{Mach} = cH_0/2\pi$ entirely from the CMB temperature and α. The fact that this thermodynamically derived scale eliminates the bias in rotation curves ($+0.53$ km/s vs > 5 km/s for MOND) serves as strong evidence that gravity is not an isolated force, but a holographic response to the global energy state.

20.1 The Unified Scale Invariance

The condition for galactic stability derived here is a direct manifestation of the same topological phase-closure constraint acting at the cosmic scale. As established in the *Prerequisite*, the fine-structure constant α defines the scaling ratio between the base state of matter and the critical limit. This implies that the macroscopic horizon R_H and the microscopic Compton wavelength λ_e are rigidly locked by the same geometry.

Therefore, the Galaxy is the gravitational realization of the Bohr orbit, scaled by the total relational capacity of the Universe.

System	**Microcosm (Atom)**	**Macrocosm (Galaxy)**
Closure Condition	Standing Wave	Horizon Resonance
Geometric Equation	$2\pi r_n = n\lambda_e$	$R_{trans} = \sqrt{\frac{3}{2}\pi R_s R_H}$
Scaling Projection	α (Kinematic Ground)	H_0 (Horizon Limit)

20.2 Final Conclusion

We have demonstrated that the "Dark Matter" phenomenon is the observational signature of scale-invariant geometric closure. By replacing the dark sector with the rigid geometry of the Global Horizon, we achieve a unification of Baryonic physics across 20 orders of magnitude.

Just as the electron must satisfy the standing wave condition to exist as a bound state within the atom, the galaxy must satisfy the frequency resonance condition to exist as a bound state within the Universe. The precision of these predictions, achieved without any free parameters, strongly suggests that the paradigm of "Dark" phenomenology is becoming obsolete, superseded by a transparent **Relational Geometric Ontology.**

Code and data are fully open-source at: https://antonrize.github.io/WILL/

References

[1] Planck Collaboration. (2020). Planck 2018 results. VI. Cosmological parameters. *Astronomy & Astrophysics*, 641, A6.

[2] Lelli, F., McGaugh, S. S., & Schombert, J. M. (2016). SPARC: Mass Models for 175 Disk Galaxies with Spitzer Photometry and Accurate Rotation Curves. *The Astronomical Journal*, 152(6), 157.

[3] Chae, K. H. (2023). Breakdown of the Newton–Einstein Standard Gravity at Low Acceleration in Internal Dynamics of Wide Binary Stars. *The Astrophysical Journal*, 952(2), 128.

[4] Hernandez, X., et al. (2023). Internal kinematics of Gaia DR3 wide binaries. *Monthly Notices of the Royal Astronomical Society*, 525(2), 2615.

[5] Bolton, A. S., et al. (2008). The Sloan Lens ACS Survey. V. The Full Sample of 70 Lens Candidates and Strong Lensing Mass Models. *The Astrophysical Journal*, 682(2), 964.

[6] Auger, M. W., et al. (2009). The Sloan Lens ACS Survey. IX. Colors, Lensing and Stellar Masses of Early-Type Galaxies. *The Astrophysical Journal*, 705(2), 1099.

[7] Li, P., Lelli, F., McGaugh, S. S., & Schombert, J. M. (2020). A Comprehensive Catalog of Dark Matter Halo Models for SPARC Galaxies. *The Astrophysical Journal Supplement Series*, 247(1), 31.

[8] Wang, D.-C., Xu, F., & Luo, X. (2020). Comparison of Modeling SPARC spiral galaxies' rotation curves with different dark matter and MOND models. *arXiv preprint arXiv:2008.04795*.

[9] Milgrom, M. (2001). MOND - A Pedagogical Review. *NED Level 5 Review*.

[10] F. Iocco, M. Pato, and G. Bertone, "Evidence for dark matter in the inner Milky Way," *Nature Physics*, vol. 11, no. 3, pp. 245–248, 2015.